Application of the X-ray micro-computed tomography to the analysis of the structure of polymeric materials

Piotr P. Szewczykowski[1), *)], Łukasz Skarżyński[2)]

DOI: dx.doi.org/10.14314/polimery.2019.1.2

Abstract: In this paper the application of X-ray micro-computed tomography (micro-CT) as a non-destructive testing method of polymeric materials is presented. Increasing applicability of polymers in varied end-use industries such as automotive, building and construction, consumer goods, and packaging is propelling the growth of the global polymer processing market. However, controlling of the polymer structure is one of the most important aspects since it affects mechanical properties of the components. The paper contains examples of two- and three-dimensional analysis of selected polymeric materials using of X-ray micro-computed tomography. Due to the complex structure of polymers, their shape and pores that are embedded inside the material and are not connected to the surface, the X-ray micro-computed tomography is an ideal solution for the analysis of the microstructure of polymeric materials to improve the process of their production in order to obtain components with the best possible properties.

Keywords: microstructure, non-destructive test, polymeric materials, X-ray micro-CT.

Zastosowanie mikrotomografii komputerowej do analizy struktury materiałów polimerowych

Streszczenie: Przedstawiono zastosowanie mikrotomografii komputerowej do bezinwazyjnej analizy struktury wewnętrznej materiałów polimerowych. Zwiększenie możliwości zastosowania polimerów w różnych branżach, takich jak: motoryzacja, budownictwo i opakowania, napędza rozwój światowego rynku przetwórstwa polimerów. Kontrola struktury materiałów, mającej ogromny wpływ na właściwości mechaniczne kompozytów polimerowych, jest bardzo istotna. Przedstawiona metoda mikrotomografii komputerowej, służąca ulepszeniu procesu wytwarzania komponentów o jak najkorzystniejszych właściwościach, jest idealnym narzędziem do analizy mikrostruktury materiałów polimerowych ze względu na ich złożoną budowę, kształt oraz liczbę porów zawartych w strukturze materiału (niestykających się z jego powierzchnią zewnętrzną). Podano przykłady dwu- i trójwymiarowej analizy mikrostruktury wybranych materiałów polimerowych z zastosowaniem mikrotomografii komputerowej.

Słowa kluczowe: mikrostruktura, badanie bezinwazyjne, materiały polimerowe, mikrotomografia komputerowa.

Materials science is interdisciplinary by nature and applications can be found in most industrial sectors, such as the automotive, building, chemical, medical, electrical, pulp, and paper industries. A distinctive feature of materials science is the search for useful relations between the structure (on different levels) and material properties. In the case of polymeric materials, the processing technology chosen and processing parameters have a very strong influence on the structure of the material and thus on its performance in a given application. Controlling the geometry of molded pieces and its structure plays a very important role since it determines the quality of final product. Most often, the porosity or samples' internal defects are investigated after breaking the specimen. The exposed cross-section is investigated visually or using scanning electron microscopy (SEM). However, there may be additional distortion of the real cross-section images in case of polymers existing at room temperature above its glass transition temperature, so lowering the temperature at breaking is necessary in this case. Recently, the application of the high-resolution X-ray computed tomography (called also micro-CT) significantly increased. It is a non-destructive technique that

[1)] UTP University of Science and Technology, Department of Materials Engineering and Polymer Processing, Faculty of Mechanical Engineering, Al. prof. S. Kaliskiego 7, 85-796 Bydgoszcz, Poland.

[2)] Gdańsk University of Technology, Department of Building Structures and Material Engineering, Faculty of Civil and Environmental Engineering, G. Narutowicza 11/12, 80-233 Gdańsk, Poland.

[*)] Author for correspondence;
e-mail: piotr.szewczykowski@utp.edu.pl

provides 3D images of the structure in materials from different life domains. Micro-computed tomography investigations are used, among others, to study the structure of tissues and organs (*e.g.*, bones, teeth, lungs) [1–3], living organisms [4], electronic devices [5], food products [6–9], geology [10–11], wood [12], *etc*. The micro-CT image analysis offers the possibility to study in detail the size and shape of each individual particle present in polymeric materials.

The main objective of this paper is to demonstrate applications of X-ray micro-computed tomography in investigations of polymers microstructure on the basis of some examples. Obtaining porous polymers by injection molding process and their porosity measurements are ones of the main specializations of the Department of Materials Science and Polymer Processing (DMS & PP) at the UTP University of Science and Technology in Bydgoszcz. Therefore, porosity measurement of polypropylene (PP) Acurell® XP 100-84 sample by using CT and comparing the results with data delivered by a producer was one of the first investigations. PP molded pieces modified by microspheres blowing agents by AkzoNobel are the other example. Microspheres are being often used at the DMS & PP since they have many applications like in packaging materials and deliver spherical pores with a diameter between 50–200 μm depending on the processing conditions and specific microspheres applied. This kind of samples was chosen for obtaining pore size distribution. MuCell® technology is an example of obtaining porous injection molded pieces by physical process. DMS & PP cooperates with a company producing large-scale elements for automotive industry and applies MuCell® technology. Samples from those elements were investigated by CT in order to obtain pore size distribution and glass fiber orientation. The last example are CT results of 3D printed inserts being placed in injection mold in order to obtain multistructural parts. Application of 3D printed inserts in injection molding technology is one of the last interests at the DMS & PP.

X-RAY MICRO-COMPUTED TOMOGRAPHY TECHNIQUE

The X-ray micro-computed tomography (called also micro-CT) is a non-destructive 3D imaging technique which uses X-rays to create cross-sections of a physical object that is used to recreate a virtual model (3D model) without destroying the original object (Fig. 1).

The pixel sizes of the cross-sections are in the micrometer range. The first prototype of X-ray micro-computed tomograph was developed by Godfrey Newbold Hounsfield. Initial application of this type of apparatus was in medical field. Prototype, constructed in 1971, was used a year later and obtained images helped to diagnose a tumor in patient's head. This invention had such a wide range of applications, that Godfrey Hounsfield and Allan McLeod Cormack, who developed a mathematical method to calculate radiation absorption in human body, received a Nobel Prize in 1979. The first system of micro-computed tomography was built by Elliott and Dover at the beginning of 1980s [13]. In general, micro-CT scanning techniques can be divided into two main groups: *in vivo* and *ex vivo*, intended for testing of living organisms and non-living objects, respectively. In the first case, the examined object is placed on a fixed "bed", which may possibly perform a sliding motion. The X-ray tube and detector are opposite to each other and move in a circular motion around the object being examined. In the second case, when examining non-living objects, usually the X-ray tube and detector are placed against each other, while the object being examined rotates around its own axis. The basic physical X-ray principal of the micro-computed tomography is the interaction of the ionizing radiation with the material, where the so-called photo-effect builds the main interaction mechanism. The photo-effect attenuates the photons proportional to the third power of the order number of the elements and inverse proportional to the

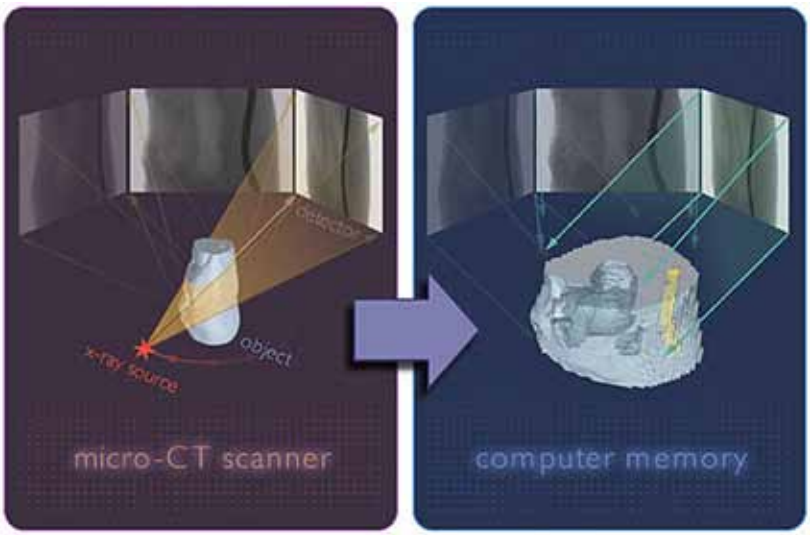

Fig. 1. Operation principle of X-ray micro-computed tomography (www.bruker-microct.com)

third power of the photon energy. As the X-ray beam penetrates an object, it is exponentially attenuated according to the material along its path. The energy-dependent material constant appearing in the exponent of the attenuation formula is called the linear attenuation coefficient. It expresses the amount of the radiation that is attenuated on an infinitely small distance in which the final attenuation reflects the sum of all these local linear attenuations along the X-ray beam. The X-ray image represents an image of the sum of all local attenuations along the X-ray beam [14]. The 3D images of the interior of an object are obtained by collecting a series of 2D images that are stored while the specimen investigated is rotated. The structures are reconstructed using the combination of all 2D cross-sections (projections) which are then used to analyze the 2D or 3D morphological parameters of the object and create a realistic visual model. The source is mostly either a microfocus X-ray tube or a device of a synchrotron radiation facility. The detector is normally based on a CCD camera with a phosphor layer to convert X-rays to a visible light.

Some artefacts are commonly encountered in micro-computed tomography and may obscure or simulate pathology. There are many different types of micro-CT artefacts, including: ring artefacts, noise, beam hardening and scatter, motion artefact, misalignment, metal artefacts, out of field artefacts and defect pixels which were discussed in detail in [15, 16].

APPLICATION OF X-RAY MICRO-CT IN POLYMERIC MATERIALS

In general, micro-computed tomography method enables to non-destructively evaluate voids, delamination phenomenon, imperfections and cracks, porosity, fiber orientation and distinguish different phases in polymeric materials and composites [17].

Porous polymers analyzed by micro-CT can reveal pore size and pore size distribution. Evans *et al.* investigated surface porous polyether-ether-ketone as orthopedic implant materials [18]. Roughness, surface porosity, distribution of open and closed pores were analyzed. Polymeric foams are often investigated by micro-CT, both at static and dynamic conditions [19–21]. There are many publications showing the porosity analysis by micro-CT of polymers for medical and scaffold applications [22], but not so much of porous polymers obtained under industrial conditions, like in case of applying gas in supercritical state as a blowing agent [23]. 3D analysis of different phases in blends composites, visualization of talk dispersion and morphology of natural fiber and wood polymer composites (WPC) are possible as well [24–26]. Diameters and orientations of celluloses fibers, *e.g.*, in polylactide (PLA) or PP matrix were wildly investigated [27–30] while Han *et al.* [31] tried to establish a correlation between density and micro-CT number in case of WPC. Dispersion and degradation of natural fibers, *e.g.*, wood fibers in PLA matrix, during polymer processing are another interesting research topic [32, 33].

In addition to natural fibers, orientation and distribution of glass fibers in injection molded materials have been presented in many publications, since its significant importance in strengthening polymeric composites [34, 35]. Simultaneous effect of fiber orientation and notches on fatigue behavior was investigated by Bernasconi *et al.* [36]. In the other paper one can see the comparison of glass fiber orientation evaluation by optical and micro-computed tomography method [37]. Micro-CT can be also used as a method confirming modeled behavior and orientation of glass fiber in injection molded samples [38, 39]. Similarly, tomography is more often used as a dimensional verification method to injection molded parts, *e.g.*, wall thickness of the injection blow molded bottles can be measured with tomography and compared with polymer processing simulation [40, 41].

Except from pores, voids and fibers distribution and orientation, micro-CT is being widely applied for damage analysis of composites [42]. For example, it can be used to apply in such important applications like observing cracks in epoxy composites used in aerospace [43]. Investigation of cracking phenomenon in laminated carbon fiber composites, damage and fracture resistance in glass fiber epoxy resin or voids being created during creep mechanism can be found in literature [44–46]. Interesting way of research is combining tensile test machine together with micro-computed tomography, which enables to perform *in situ* test, *e.g.*, breaking mechanism of PA66 composites reinforced with short glass fiber or influence of humidity on PA6 damage mechanism between fibers and matrix [47, 48]. Similar technique but joined with volumetric digital image correlation was applied to investigate other composites, like deformations in CFRP [49, 50]. There are many other *in situ* experiments and applications summarized by Buffiere *et al.* [51]. Some tests were carried out on samples, which were stopped before failure during tensile tests and necks were investigated by micro-CT [52].

Recently, dynamically developing rapid prototyping technologies became another field of applications for micro-computed tomography investigations. In case of fused deposition modeling (FDM) the precision of building the polymer layers and adhesion between filaments influence the quality and mechanical properties of printed element. Imperfections and voids are weakening the product and micro-computed tomography enables to analyze the final product [53, 54]. It should be mentioned, that micro-computed tomography has many applications in investigating polymeric and composites' materials used in stomatology, for example in evaluation of bonding between polymeric cements and tooth in dental applications [55, 56].

EXPERIMENTAL EXAMPLES

This part presents some applications of X-ray micro-computed tomography in analysis of the microstructure

of polymeric materials. An explanation of choosing the following examples is presented earlier. Samples of microporous polypropylene (PP) Acurell® XP 100-84, polypropylene (PP) with the addition of blowing agent in the form of microspheres were investigated using SkyScan 1272. Polyamide 6 (PA6) samples with the addition of glass fiber that were obtained using MuCell® technology and samples printed in the incremental technology were scanned using SkyScan 1173.

Microtomography apparatus

X-ray micro-computed tomograph Skyscan 1272 and prototype extended X-ray micro-computed tomograph Skyscan 1173 (Fig. 2) were used. Both scanners are particularly advantageous at intermediate resolution levels, where scans are completed up to ten times faster with the same resolution and image quality, compared to previous micro-CTs with a fixed source-detector design. Scanners are equipped with the newly developed 130 keV and 100 keV microfocus, X-ray source for SkyScan 1173 and 1272, respectively, with a very stable focal spot position, flat panel sensor of a large format (up to 11 Mpx) with a special protection by a lead-glass fibre-optic window. The scanners are additionally equipped with a precision object manipulator which allows for a very precise and automatic specimen positioning. Both scanners have several filters available in the front of the X-ray detector: 0.25 mm brass filter, 1.0 mm aluminum filter, 2.0 mm lead filter and 0.25 mm copper filter. As compared to usual micro-computed tomographs, there is one main advantage of our apparatus Skyscan 1173: large specimens up to 300 mm in diameter may be scanned (using an oversize function).

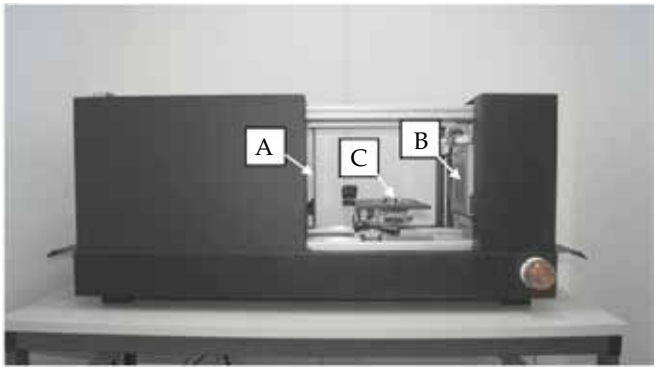

Fig. 2. X-ray micro-computed tomograph Skyscan 1173: A) X-ray source, B) flat panel, C) precision object manipulator

Samples of microporous polypropylene Acurell® XP 100-84

Porous polypropylene carrier Acurell® XP 100-84 (Fig. 3) was scanned by Bruker SkyScan 1272 micro-computed tomograph in order to compare analyzed total porosity with data presented by the producer. Accordingly to product data sheet the pores content should be on the level 84 ± 5 %.

Scanning parameters for the sample: source voltage 35 kV, source current 200 μA, image pixel size 2 μm, exposure 1780 ms, rotation step 0.3°, frame averaging 4 and

a) b)

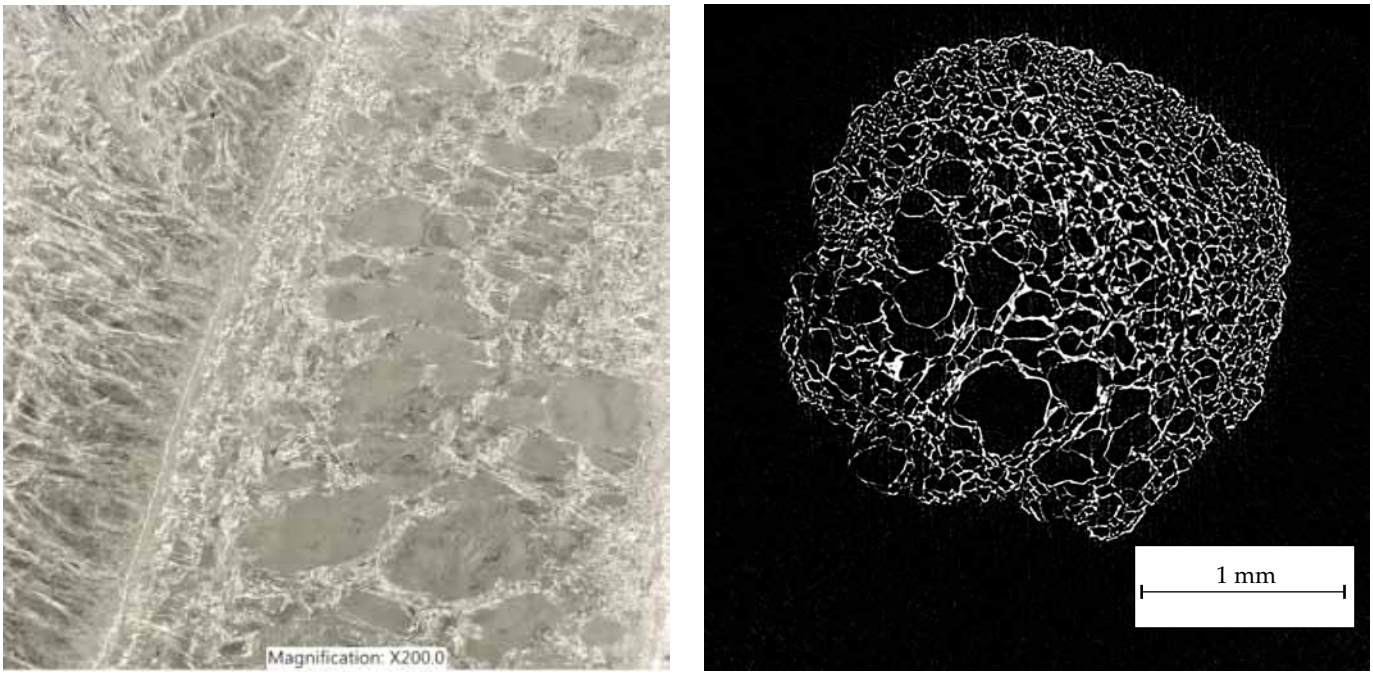

Fig. 3. Pictures of microporous polypropylene Acurell® XP 100-84 obtained by: a) digital microscope Keyence VHX 6000, 200× magnification, b) micro-computed tomograph SkyScan 1272 by Bruker; picture presents cross-section (approximately 2.6 mm in diameter) of investigated sample with scanning resolution of 2 μm

random movement 10. The reconstructed cross-section in the middle height of the scanned sample is presented in Fig. 3. All cross-sections were analyzed in CTAn software and 3D analysis showed that total porosity of polypropylene was approximately 84.87 %. This value was obtained by CTAn software after binarization of the reconstructed layers of the object. Each pixel of the image is recorded in a grey scale in a range of values from 0 to 255. For purpose of morphometric analysis each pixel needs to become white or black. Therefore a threshold value on the histogram needs to be established to define which pixels (in 2D) or voxels (in 3D) should be black (recognized as pores) or white (recognize as bulk material). The disadvantage is the subjective method of establishing this value, which influences the final result of calculated porosity. The aim of investigating PP Acurell® sample was to determine the consistency of total porosity value obtained by CT measurements with values delivered by the producer. Similar results confirmed correctness of applied reconstruction and data analysis procedure.

Microspheres as a polypropylene blowing agent

3 % by weight of microspheres 930 MB 120 by Akzo Nobel was pre-mixed with polypropylene Moplen HP500N by Basell Orlen Polyolefins. Material was injected by ENGEL e-victory 310/110 hybrid injection molding machine, polymer processing conditions were as follow: polymer melt temperature: 200 °C, injection mold temperature: 30 °C, no holding phase. Sample was scanned by using Bruker SkyScan 1272 with the following scanning parameters: source voltage 40 kV, source current 200 μA, image pixel size 3.5 μm, exposure 670 ms, rotation step 0.3°, frame averaging 3 and random movement 40. Figure 4a presents a single layer after tomographic reconstruction, where dark spots represent pores obtained by microspheres. In order to perform the 3D analysis and obtain pore size ranges distribution images need to be binarized – image composed of only white and dark spots, which represent bulk material and pores, respectively (Fig. 4b).

After this operation there are many artefacts like white spots inside big pores and numerous tiny black spots in bulk material, therefore a despeckle operation needs to be carried out (Fig. 4c). Final plot pore distribution is presented in Fig. 5.

Obtained results show the highest amount, on the level of 20 %, for pore size in range between 0.108 and 0.143 mm. Presented results are part of the expanded experiment in which the influence of microspheres concentration and the addition of a nucleating agent on the pore size distribution was investigated. Completed data are going to be presented in a separate publication.

MuCell® polyamide samples

Samples were cut from large-scale element from PA6 reinforced with 30 wt % of glass fiber. Molded pieces were obtained in injection molding technology com-

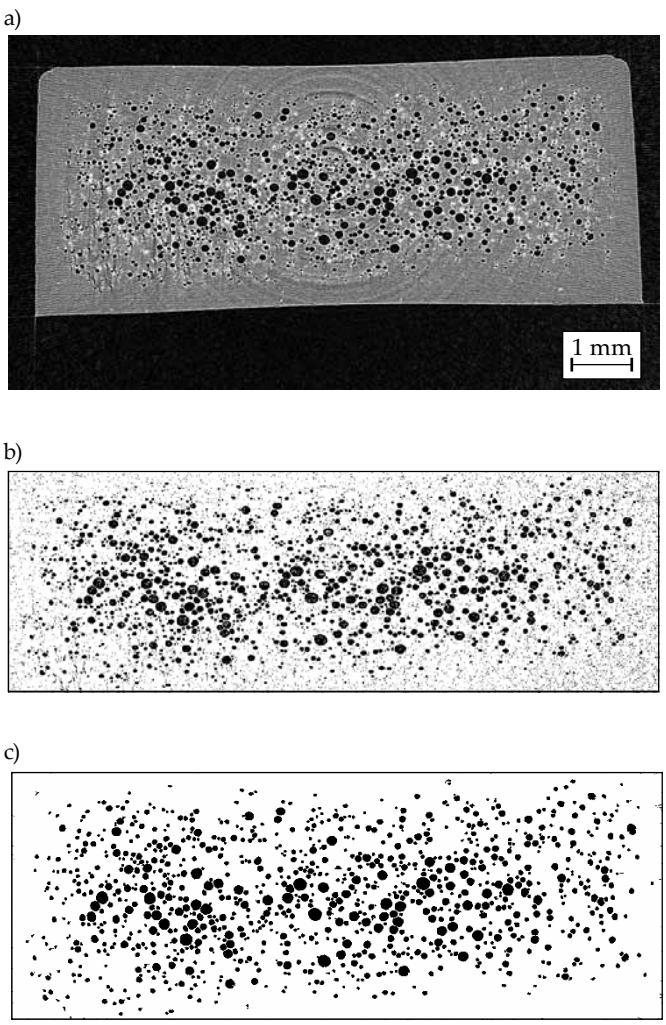

Fig. 4. Pictures of: a) 2D visualization of a single layer of microporous polypropylene with microspheres, b) picture after cropping the region of interest and binary selection, c) the same picture after binarization of the image and removing white and dark spots by despeckle operation; pictures obtained by Bruker micro-computed tomograph SkyScan 1272

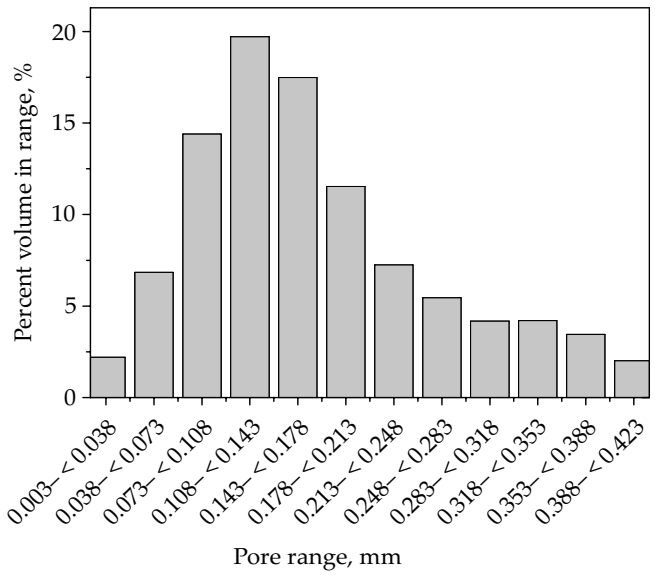

Fig. 5. Pore size ranges distribution for porous PP sample; pores with percent volume in range less than 1 % were neglected

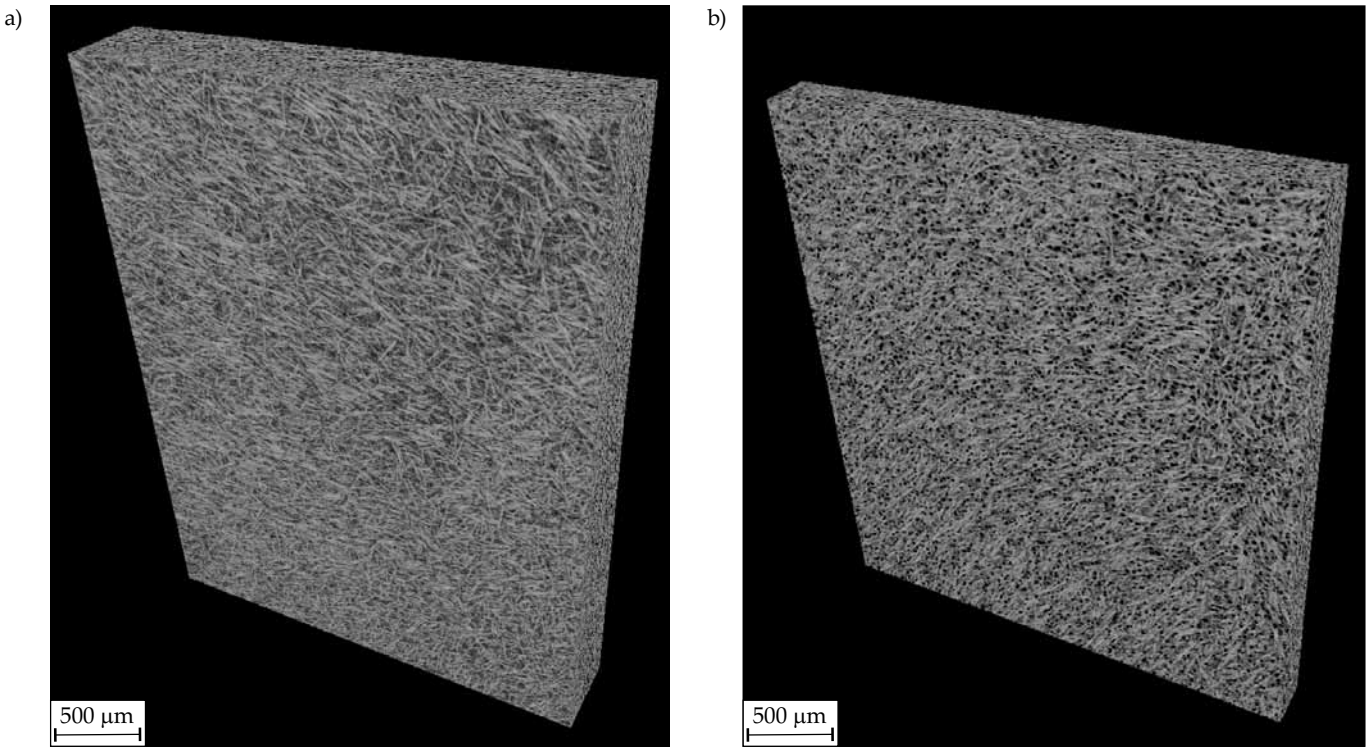

Fig. 6. 3D images of the MuCell polyamide sample: a) outer surface, b) cross-section; black color represents pores

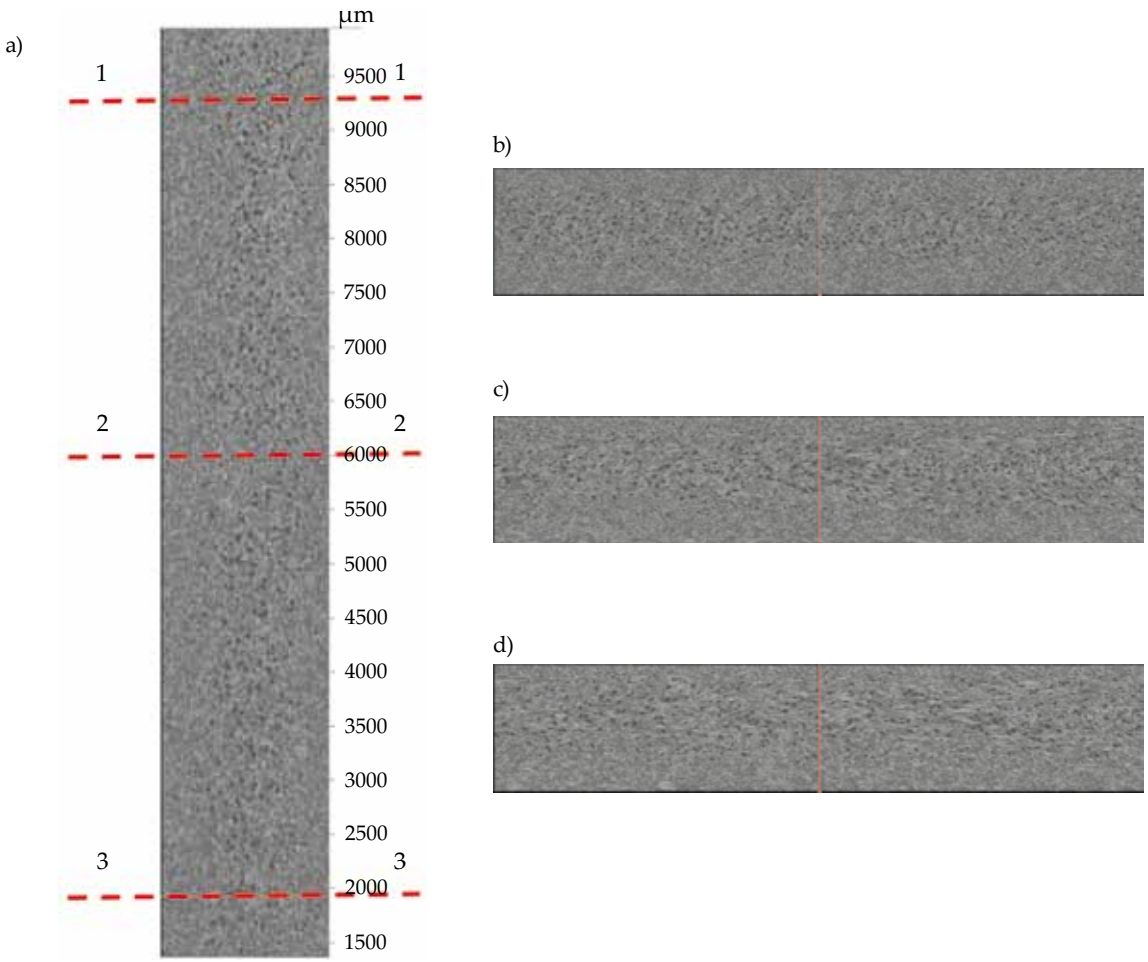

Fig. 7. 3D images of the MuCell polyamide sample: a) vertical cross-section in the middle of the sample thickness, b), c), d) horizontal cross-sections across the lines 1-1, 2-2 and 3-3, respectively; black color represents pores

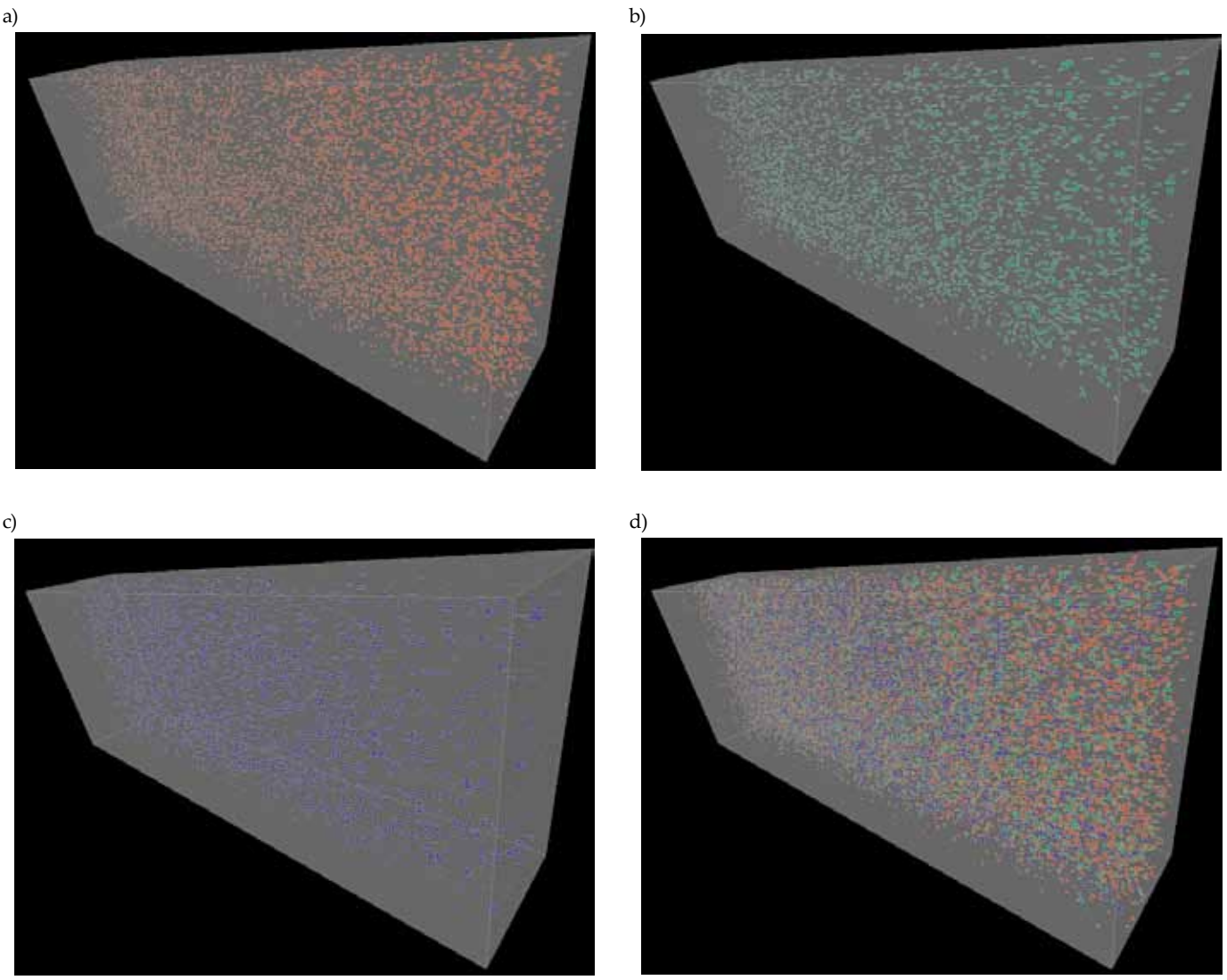

Fig. 8. Distribution of pores size in polyamide specimen (cross-section 1.5 × 8.0 mm, height 6.0 mm) by structure thickness analysis in micro-computed tomography: a) pores size 0–50 μm, b) pores size 50–75 μm, c) pores size > 75 μm, d) all pores

bined with installation with nitrogen in supercritical state, which works as a blowing agent (microcellular MuCell® injection molding technology). In presented example large-scale element was injection molded with 3 wt % of nitrogen. From the large-scale molded pieces three samples were cut out: one which was in a close distance to the gate (Gd1) and two samples in a far distance from the gate (Gd2 and Gd3). Micro-computed tomography was performed in order to obtain pore size ranges and their distribution and to observe glass fiber orientation.

Samples were approximately 15 mm high, 10 mm wide and 2 mm thick. During tests the X-ray source voltage of the micro-CT scanner was set to 50 keV, the current to 160 μA, the exposure time to 500 ms, rotation step was 0.4° (total rotation 180°), frame averaging was 4, random movement was 10 and no filter was used. Pixel size was 5.2 μm and scanning time was about 35 min. The structures were reconstructed using the combination of all 2D cross-sections (projections) with smoothing (using Gaussian distribution), ring artefact reduction and beam

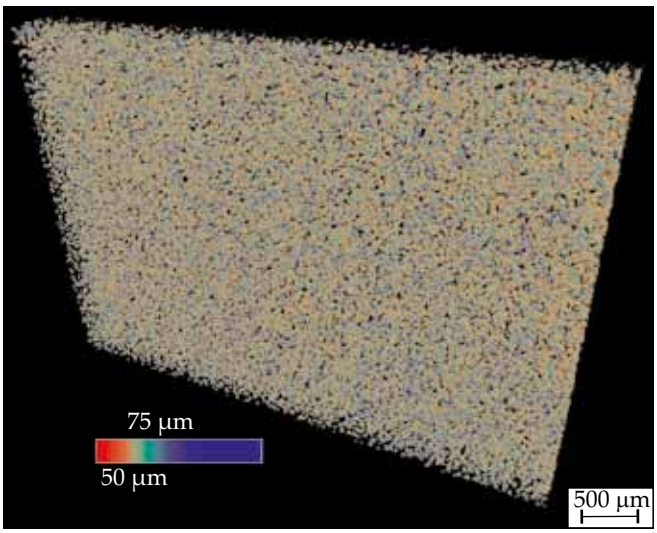

Fig. 9. 3D distribution of pores in polyamide specimen by structure thickness analysis in micro-computed tomography

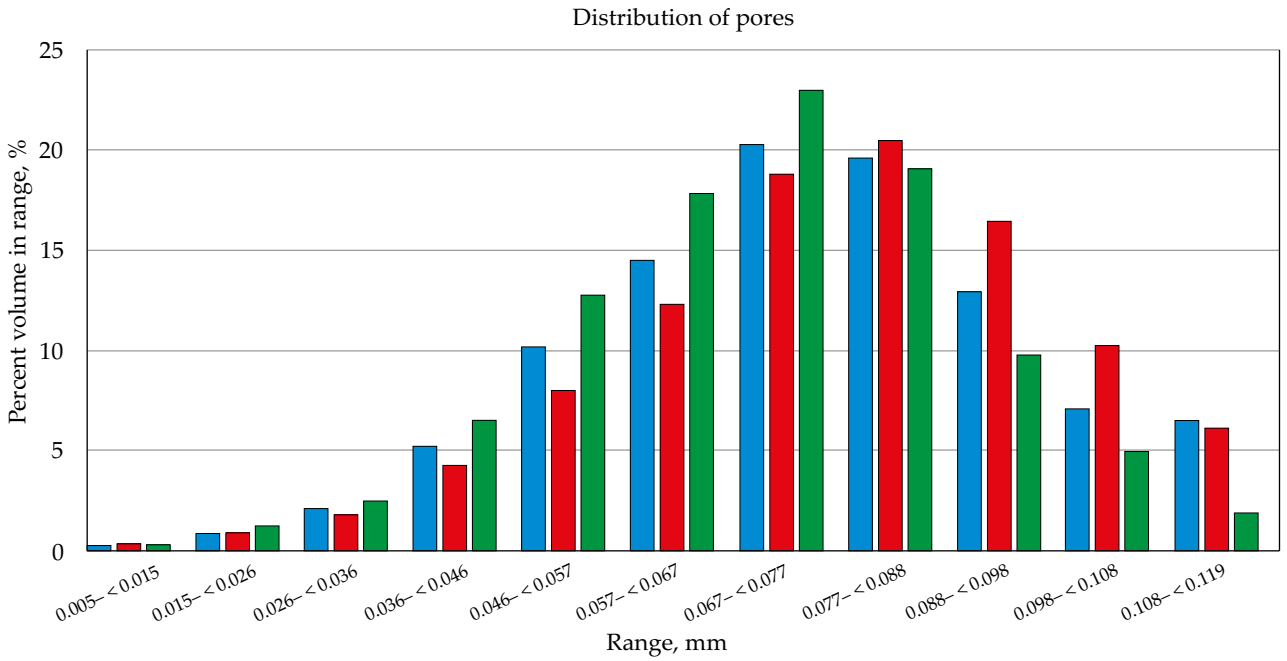

Fig. 10. Distribution of pores in polyamide specimen: Gd1 (blue bars), Gd2 (red bars), Gd3 (green bars)

hardening. To preserve the problems with eccentricity of sample rotation misalignment compensation option was introduced.

Figure 6 demonstrates the 3D images of the scanned sample. Figure 6a presents the outer surface of the entire sample and Fig. 6b presents the vertical cross-section. Black dots represent pores that are randomly distributed in the entire sample. Figure 6 shows that it is difficult to obtain accurate images for glass fiber due to insufficient resolution of the apparatus. It is much easier to obtain appropriate images for fibers with a larger diameter than the diameter of glass fiber. Figure 7 shows vertical cross-section made in the center of the sample width (Fig. 7a) and corresponding horizontal cross-sections made at the bottom (Fig. 7d), at the center (Fig. 7c) and at the top (Fig. 7b) of the sample height. Different concentration and distributions of pores can be noticed.

Figure 8 presents the distribution of different size of pores: 0–50 μm (Fig. 8a), 50–75 μm (Fig. 8b), > 75 μm (Fig. 8c) and distribution of all pores (Fig. 8d). Figure 9 shows 3D distribution pores in polyamide specimen by structure thickness analysis in micro-computed tomography. Both Figs. 8 and 9 are attached in order to present possibilities of separation of pores with a given diameter range in 3D space. Figure 10 presents distribution of pores of different size in samples marked Gd1, Gd2 and Gd3. At the point closest to the gate, the pores in the 67–77 μm range dominate, similarly for the point Gd3. The peak of pore size distribution for the point Gd2, which is the furthest from the gate, is clearly shifted towards the pores with a larger diameter, in the range of 77–80 μm. The explanation of the difference in pore size between Gd2 and Gd3 points would require additional analysis of polymer flow length which was not the subject of this article. Larger pore sizes for the most distant Gd2 point may be due to a drop pressure and since better conditions for pore growth.

Samples prepared by 3D printing process

Samples for tensile tests were prepared by fused filament fabrication (FFF), one of the most popular 3D printing process, with use of Mark II 3d printer by Markforged. Samples are reinforced with filament glass fiber which

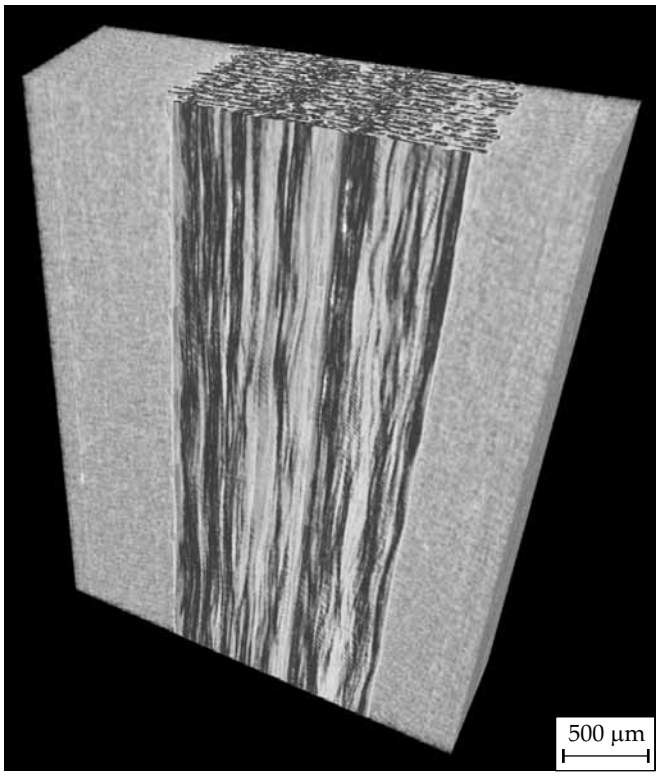

Fig. 11. 3D visualization of printed sample with filament glass fiber in the central part

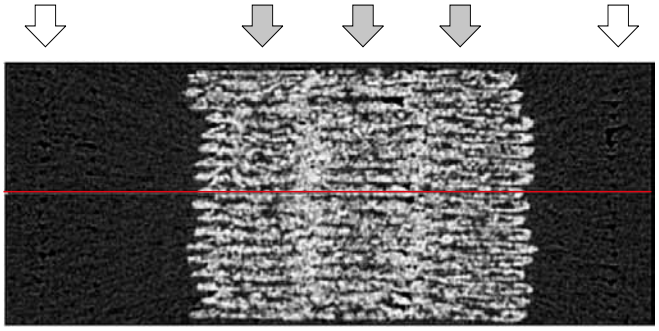

Fig. 12. Visualization of printed sample cross-section with assumed center line of filament glass fiber marked with dark arrows and area of joining two PA filaments with visible pores marked with light arrows

was extruded with the second head. The basic, matrix material is called ONYX by Markforged, which is PA reinforced with short cut carbon fiber. Figure 11 presents a 3D scan of such sample, where filament glass fiber is in the middle part. In Fig. 12 center line of filament glass fiber is marked with dark arrows. This filament is most probably in its own matrix, which melts in the 3D printer head and enables adhesion between filament layers. In the picture it is seen, that this filament is squeezed in the printing process. White arrows present area of joint PA filament without glass fiber with visible pores. All those spaces are weakening points and will influence the tensile strength and impact resistance of 3D printed elements like inserts for injection molded pieces. CT enables non-destructive verification of such inserts before placing it in the injection mold. Correlation between distribution of pores in 3D printed inserts verified by CT and its mechanical properties will be presented in a separate publication.

CONCLUSIONS

The following conclusions can be drawn from the literature studies and experiments with polymeric materials:

– X-ray micro-computed tomography is a powerful tool for the visualization and quantification of polymeric materials structure. The 3D distribution and size measurement of pores can be achieved.

– Micro-computed tomography technique allowed for detailed analysis of pores size and pores distribution. Total porosity measured in polypropylene carrier Acurell® XP 100-84 was 84.87 %, measurements precision was ± 0.5 %, while, according to product data sheet, the pore content should be on the level 84 ± 5 %. Pore size, pore size distribution as well as fibers orientation can be estimated for porous PP and PA6 samples, however proper data reduction is necessary in order to avoid misinterpretations. Imperfections and pores in 3D printed elements can be easily reviled as well.

– Some of the disadvantages of CT methods are high cost of apparatus, necessary high computing power to operate the data, personnel high skills to interpret and prepare the 3D visualizations correctly and longtime of data handling which increases with higher resolution of obtained images.

FUTURE PERSPECTIVES

Our experiments will be continued. More advanced quantitative analysis of the polymeric materials will be carried out. Additionally, the servo-testing machine INSTRON 5569 that is equipped with a special load handle which will allow for the specimen rotation during deformation. The successive 3D images during deformation (compression and bending) will be obtained and analyzed.

REFERENCES

[1] Pauwels E., Van Loo D., Cornillie P. *et al.*: *Journal of Microscopy* **2013**, *250*, 21. http://dx.doi.org/10.1111/jmi.12013
[2] Bannerman A., Paxton J.Z., Grover L.M.: *Biotechnology Letters* **2014**, *36*, 403. http://dx.doi.org/10.1007/s10529-013-1374-4
[3] Svensson C.M., Hoffmann B., Irmler I.M. *et al.*: *Scientific Reports* **2017**, *7*, 1. http://dx.doi.org/10.1038/srep44434
[4] Onelli O., Kamp T., Skepper J. *et al.*: *Scientific Reports* **2017**, *7*, 1. http://dx.doi.org/10.1038/s41598-017-01496-8
[5] Channagiri S.A., Nagpure S.C., Babu S.S. *et al.*: *Journal of Power Sources* **2013**, *243*, 750. http://dx.doi.org/10.1016/j.jpowsour.2013.06.023
[6] Cantre D., Herremans E., Verboven P. *et al.*: *Innovative Food Science and Emerging Technologies* **2014**, *24*, 28. http://dx.doi.org/10.1016/j.ifset.2013.12.008
[7] Laverse J., Mastromatteo M., Frisullo P., Del Nobile M.A.: *Journal of Dairy Science* **2011**, *94*, 43. http://dx.doi.org/10.3168/jds.2010-3524
[8] Mathieu V., Monnet A.F., Jourdren S. *et al.*: *Food & Function* **2016**, *7*, 3577. http://dx.doi.org/10.1039/C6FO00522E
[9] Alam T., Takhar P.S.: *Journal of Food Science* **2016**, *81*, 651. http://dx.doi.org/10.1111/1750-3841.13219
[10] Bubeck A., Walker R.J., Healy D. *et al.*: *Earth and Planetary Science Letters* **2017**, *457*, 38. http://dx.doi.org/10.1016/j.epsl.2016.09.050
[11] Otani J., Watanabe Y., Chevalier B.: *IOP Conference Series: Materials Science and Engineering* **2010**, *10*, 1. http://dx.doi.org/10.1088/1757-899X/10/1/012089
[12] Joffre T., Isaksson P., Dumont P.J.J. *et al.*: *Experimental Mechanics* **2016**, *56*, 723. http://dx.doi.org/10.1007/s11340-015-0119-9
[13] Elliott J.C., Dover S.D.: *Journal of Microscopy* **1982**, *126*, 211. https://doi.org/10.1111/j.1365-2818.1982.tb00376.x
[14] http://www.b-cube.ch (access date 14.02.2018)
[15] Boas F.E., Fleischmann D.: *Imagining in Medicine* **2012**, *4*, 229. http://dx.doi.org/10.2217/iim.12.13

[16] Skyscan NV (2011) Nrecon User Manual 4/20/2011.
[17] Bossi R.H., Georgeson G.E.: *Materials Evaluation* **1995**, *53*, 1198.
[18] Evans N.T., Irvin C.W., Safranski D.L., Gall K.: *Journal of the Mechanical Behavior of Biomedical Materials* **2016**, *59*, 459. http://dx.doi.org/10.1016/j.jmbbm.2016.02.033
[19] Elmoutaouakkil A., Fuchs G., Bergounhon P. *et al*.: *Journal of Physics D: Applied Physics* **2003**, *36*, A37. http://dx.doi.org/10.1088/0022-3727/36/10A/308
[20] Viot P., Bernard D., Plougonven E.: *Journal of Materials Science* **2007**, *42*, 7202. http://dx.doi.org/10.1007/s10853-006-1422-8
[21] Smolná K., Gregor T., Kosek J.: *European Polymer Journal* **2013**, *49*, 3966. http://dx.doi.org/10.1016/j.eurpolymj.2013.08.030
[22] Lin A.S.P., Barrows T.H., Cartmell S.H. *et al*.: *Biomaterials* **2003**, *24*, 481. http://dx.doi.org/10.1016/S0142-9612(02)00361-7
[23] Wu H.B., Haugen H.J., Wintermantel E.: *Journal of Cellular Plastics* **2012**, *48*, 141. http://dx.doi.org/10.1177/0021955X11432970
[24] Pyun A., Bell J.R., Won K.H.: *Macromolecules* **2007**, *40*, 2029. http://dx.doi.org/10.1021/ma062635+
[25] Kocic N., Kretschmer K., Bastian M., Heidemeyer P.: *Journal of Applied Polymer Science* **2012**, *126*, 1207. http://dx.doi.org/10.1002/app.36880
[26] Salasinska K., Polka M., Gloc M. *et al*.: *Polimery* **2016**, *61*, 255. http://dx.doi.org/10.14314/polimery.2016.255
[27] Di Giuseppe E., Castellani R., Dobosz S. *et al*.: *Composites Part A: Applied Science and Manufacturing* **2016**, *90*, 320. http://dx.doi.org/10.1016/j.compositesa.2016.07.020
[28] Awal A., Rana M., Sain M.: *Mechanics of Materials* **2015**, *80*, 87. http://dx.doi.org/10.1016/j.mechmat.2014.09.009
[29] Graupner N., Beckmann F., Wilde F.: *Journal of Materials Science* **2014**, *49*, 450. http://dx.doi.org/10.1007/s10853-013-7724-8
[30] Alemdar A., Zhang H., Sain M.: *Advanced Engineering Materials* **2008**, *10*, 126. http://dx.doi.org/10.1002/adem.200700232
[31] Han Y., Qi D.W., Guan S.Y.: *Advanced Materials Research* **2012**, *428*, 57. http://dx.doi.org/10.4028/www.scientific.net/AMR.428.57
[32] Sliwa F., El Bounia N.E., Charrier F.: *Composites Science and Technology* **2012**, *72*, 1733. http://dx.doi.org/10.1016/j.compscitech.2012.07.002
[33] Joffre T., Miettinen A., Berthold F.: *Composites Science and Technology* **2014**, *105*, 127. http://dx.doi.org/10.1016/j.compscitech.2014.10.011
[34] Nguyen Thi T.B., Morioka M., Yokoyama A.: *Journal of Materials Processing Technology* **2015**, *219*, 1. http://dx.doi.org/10.1016/j.jmatprotec.2014.11.048
[35] Ayadi A., Nouri H., Guessasma S.: *Composite Structures* **2015**, *125*, 277. http://dx.doi.org/10.1016/j.compstruct.2015.02.005
[36] Bernasconi A., Cosmi F., Zappa E.: *Strain* **2010**, *46*, 435. http://dx.doi.org/10.1111/j.1475-1305.2009.00667.x
[37] Bernasconi A., Cosmi F., Hine P.J.: *Composites Science and Technology* **2012**, *16*, 2002. http://dx.doi.org/10.1016/j.compscitech.2012.08.018
[38] Kleindel S., Salaberger D., Eder R.: *International Polymer Processing* **2015**, *30*, 366. http://dx.doi.org/10.3139/217.3047
[39] Nciri M., Notta-Cuvier D., Lauro F. *et al*.: *Composite Structures* **2017**, *160*, 516. http://dx.doi.org/10.1016/j.compstruct.2016.10.083
[40] Ontiveros S., Yagüe-Fabra J.A., Jiménez R.: *Measurement Science and Technology* **2012**, *23*, 1. http://dx.doi.org/10.1088/0957-0233/23/12/125401
[41] Biglione J., Bereaux Y., Charmeau J.Y.: "Injection blow moulding single stage process: Validation of the numerical simulation through tomography analysis" AIP Conference Proceedings, Nantes, France 2016, vol. 1769, 020012. http://dx.doi.org/10.1063/1.4963416
[42] Masters J.E.: *American Society for Testing and Materials* **1992**, 35. http://dx.doi.org/10.1520/STP1128-EB
[43] Wright P., Fu X., Sinclair I. *et al*.: *Journal of Composite Materials* **2008**, *42*, 1993. http://dx.doi.org/10.1177/0021998308092211
[44] ElAgamy N., Laliberté J., Gaidies F.: *Journal of Composite Materials* **2016**, *50*, 2523. http://dx.doi.org/10.1177/0021998315608252
[45] Sket F., Seltzer R., Molina-Aldareguía J.M.: *Composites Science and Technology* **2012**, *72*, 350. http://dx.doi.org/10.1016/j.compscitech.2011.11.025
[46] Selles N., Saintier N., Laiarinandrasana L.: *International Journal of Plasticity* **2016**, *86*, 112. http://dx.doi.org/10.1016/j.ijplas.2016.08.004
[47] Rolland H., Saintier N., Robert G.: *Composites Part B: Engineering* **2016**, *90*, 365. http://dx.doi.org/10.1016/j.compositesb.2015.12.021
[48] Arif M.F., Meraghni F., Chemisky Y.: *Composites Part B: Engineering* **2014**, *58*, 487. http://dx.doi.org/10.1016/j.compositesb.2013.11.001
[49] Croom B., Wang W.M., Li J., Li X.: *Experimental Mechanics* **2016**, *56*, 999. http://dx.doi.org/10.1007/s11340-016-0140-7
[50] Safriet S., Quick T., Mollenhauer D. *et al*.: "Three--Dimensional Analysis of Damage Propagation in Unidirectional Polymer Composites using X-ray Computed Tomography and Digital Volume Correlation", 30th Technical Conference of the American Society for Composites **2015**, 2449.
[51] Buffiere J.Y., Maire E., Adrien J. *et al*.: *Proceedings of the Society for Experimental Mechanics, Inc.* **2010**, *67*, 289.
[52] Laiarinandrasana L., Morgeneyer T.F., Proudhon H., Regrain C.: *Journal of Polymer Science, Part B: Polymer Physics* **2010**, *48*, 1516.

https://doi.org/10.1002/polb.22043
[53] Nouri H., Guessasma S., Belhabib S.: *Journal of Materials Processing Technology* **2016**, *234*, 113. http://dx.doi.org/10.1016/j.jmatprotec.2016.03.019
[54] Gapinski B., Wieczorowski M., Grzelka M.: *Polimery* **2017**, *62*, 53. http://dx.doi.org/10.14314/polimery.2017.053
[55] Wagner L., Ponto-Wolska M., Raszewski Z.: *Polimery* **2016**, *61*, 831. http://dx.doi.org/10.14314/polimery.2016.831
[56] Wagner L., Ponto-Wolska M., Raszewski Z.: *Polimery* **2017**, *62*, 875. http://dx.doi.org/10.14314/polimery.2017.875
Received 14 II 2018.